Author Manuscript

Author Manuscript

Author Manuscript

Author Manuscript

HHS Public Access

Author manuscript

J Control Release. Author manuscript; available in PMC 2022 May 10.

Published in final edited form as:

J Control Release. 2021 May 10; 333: 339–351. doi:10.1016/j.jconrel.2021.03.022.

Browning white adipose tissue using adipose stromal cell-targeted resveratrol-loaded nanoparticles for combating obesity

Yujiao Zu[1], **Ling Zhao**[2], **Lei Hao**[1], **Yehia Mechref**[3,4], **Masoud Zabet-Moghaddam**[4,5], **Peter A. Keyel**[5], **Mehrnaz Abbasi**[1], **Dayong Wu**[6], **John A. Dawson**[1,4], **Ruiwen Zhang**[7], **Shufang Nie**[1], **Naima Moustaid-Moussa**[1], **Mikhail G. Kolonin**[8], **Alexes C. Daquinag**[8], **Luis Brandi**[9], **Irfan Warraich**[9], **Susan K. San Francisco**[4], **Xiaocun Sun**[10], **Zhaoyang Fan**[11,12], **Shu Wang**[1,13,*]

[1]Department of Nutritional Sciences, Texas Tech University, Lubbock, Texas 79409, USA.

[2]Department of Nutrition, The University of Tennessee, Knoxville, Tennessee 37996, USA.

[3]Department of Chemistry and Biochemistry, Texas Tech University, Lubbock, Texas 79409, USA.

[4]Center for Biotechnology and Genomics, Texas Tech University, Lubbock, Texas 79409, USA.

[5]Department of Biological Sciences, Texas Tech University, Lubbock, Texas 79409, USA.

[6]Nutrition Immunology Laboratory, Jean Mayer USDA Human Nutrition Research Center on Aging, Tufts University, Boston, Massachusetts 02111, USA.

[7]Department of Pharmacological and Pharmaceutical Sciences and Drug Discovery Institute, University of Houston, Houston, Texas 77204, USA.

[8]The Brown Foundation Institute of Molecular Medicine for the Prevention of Human Diseases, The University of Texas Health Science Center at Houston, Houston, Texas 77030, USA

[*]**To whom correspondence should be addressed:** Dr. Shu Wang, Department of Nutritional Sciences, Texas Tech University, 1301 Akron Avenue, Lubbock, TX 79409-1240, USA, Telephone number: (806) 834-4050, shuwangbao@gmail.com.

Credit author statement

Shu Wang: Funding acquisition, Supervision, Writing - Review & Editing, Conceptualization, Resources, Methodology
Yujiao Zu: Project administration, Visualization, Writing - Original Draft, Writing - Review & Editing, Methodology, Investigation
Ling Zhao: Resources, Supervision,Investigation, Writing - Review & Editing
Lei Hao: Resources, Supervision, Investigation, Review & Editing
Yehia Mechref: Resources, Methodology, Investigation, Review
Masoud Zabet-Moghaddam: Resources, Methodology, Investigation, Review Peter A. Keyel: Supervision, Resources, Formal analysis, Software, Writing - Review & Editing, Validation
Mehrnaz Abbasi: Investigation, Review
Dayong Wu: Resources, Methodology, Investigation, Writing - Review & Editing John A. Dawson: Data Curation, Formal analysis, Software, Review
Ruiwen Zhang: Conceptualization, Data Curation, Review
Shufang Nie: Methodology and Review
Naima Moustaid-Moussa: Resources and Review
Mikhail G. Kolonin: Conceptualization, Resources, Review
Alexes C. Daquinag: Conceptualization, Review
Luis Brandi: Resources, Methodology, Investigation, Review
Irfan Warraich: Resources, Methodology, Investigation, Review
Susan K. San Francisco: Resources, Review
Xiaocun Sun: Data Curation, Review
Zhaoyang Fan: Data Curation, Conceptualization, Writing - Review & Editing

Publisher's Disclaimer: This is a PDF file of an unedited manuscript that has been accepted for publication. As a service to our customers we are providing this early version of the manuscript. The manuscript will undergo copyediting, typesetting, and review of the resulting proof before it is published in its final form. Please note that during the production process errors may be discovered which could affect the content, and all legal disclaimers that apply to the journal pertain.

Author Manuscript Author Manuscript Author Manuscript Author Manuscript

[9]Department of Pathology, Texas Tech University Health Sciences Center, Lubbock, TX 70430, USA

[10]Research Computing Support, University of Tennessee, Knoxville, Tennessee 37996, USA

[11]Department of Electrical & Computer Engineering and Nano Tech Center, Texas Tech University, Lubbock, Texas 79409, USA.

[12]School of Electrical, Computer and Energy Engineering, Arizona State University, Tempe, Arizona 85287, USA.

[13]College of Health Solutions, Arizona State University, Phoenix, Arizona 85004, USA.

Abstract

Enhancing thermogenic energy expenditure via promoting the browning of white adipose tissue (WAT) is a potential therapeutic strategy to manage energy imbalance and the consequent comorbidities associated with excess body weight. Adverse effects and toxicities of currently available methods to induce browning of WAT have retarded exploration of this promising therapeutic approach. Targeted delivery of browning agents to adipose stromal cells (ASCs) in subcutaneous WAT to induce differentiation into beige adipocytes may overcome these barriers. Herein, we report for the first time, ASC-targeted delivery of trans-resveratrol (R), a representative agent, using ligand-coated R-encapsulated nanoparticles (L-Rnano) that selectively bind to glycanation site-deficient decorin receptors on ASCs. After biweekly intravenous administration of L-Rnano to obese C57BL/6J mice for 5 weeks targeted R delivery significantly induced ASCs differentiation into beige adipocytes, which subsequently resulted in 40% decrease in fat mass, accompanied by improved glucose homeostasis and decreased inflammation. Our results suggest that the ASC-targeted nanoparticle delivery of browning agents could be a transformative technology in combating obesity and its comorbidities with high efficacy and low toxicity.

Keywords

obesity; adipose stromal cells; *trans*-resveratrol; beige adipocytes; nanoparticles

1. Introduction

Obesity is a global epidemic. When energy intake exceeds expenditure, excess energy is stored in the form of fat in adipose tissue, and weight gain occurs [1]. Obesity is a key risk factor for type 2 diabetes, cardiovascular disease, sleep apnea, and some types of cancer [2]. Current anti-obesity medical therapies include pharmacotherapy and weight loss surgery; the latter approach has high efficacy but is very invasive and expensive. Pharmacotherapy often utilizes orally administered drugs. Most FDA approved drugs target energy intake either by suppressing appetite (e.g., phentermine) or by decreasing nutrient absorption (e.g., orlistat). Orally administered drugs have the highest compliance but are beset with major problems such as a high level of hepatic metabolism (the first-pass effect) and lack of target specificity, leading to a high level of side effects and toxicity. Obesity relapse may also occur when drugs are stopped. Better approaches to combating obesity are urgently needed.

Author Manuscript Author Manuscript Author Manuscript Author Manuscript

Both white adipose tissue (WAT) and brown adipose tissue (BAT) are found in mammals. WAT is the major site for energy storage, and BAT plays an important role in thermogenic energy expenditure [3, 4]. The expanded WAT in obesity is recognized as an active endocrine and inflammatory organ, typically associated with infiltration of pro-inflammatory immune cells, and excessive release of cytokines/chemokines such as tumor necrosis factor α (TNF-α) and interleukin-6 (IL-6), leptin as well as free fatty acids into circulation, many of which negatively impact whole body metabolism [5]. In contrast, BAT is positively associated with thermogenic energy expenditure and negatively associated with adiposity [6]. It also serves as a "metabolic sink" for burning free fatty acids [7], glucose, and other metabolites [8]. BAT develops less pro-inflammatory response than WAT [9]. Although BAT has been suggested as a therapeutic target for treating obesity [10], many adults do not possess active BAT [11]. Especially obese adults [12]. Even in adults with BAT, it decreases and disappears with aging [13].

Beige/brown-like adipocytes have the thermogenic function and other characteristics of the classic brown adipocytes [14]. Both beige and brown adipocytes express uncoupling protein 1 (UCP-1) in the inner mitochondrial membrane, which can dissipate the proton electrochemical gradient generated in the form of heat [15]. In contrast to classical brown adipocytes, beige adipocytes are inducible via the *de novo* differentiation of adipose stromal stem cells (ASCs) [16, 17] or transformation of white adipocytes [18]. Subcutaneous WAT is easier to access and more responsive to browning agents than visceral WAT [19]. Therefore, browning of subcutaneous WAT via enhancing ASCs differentiation to beige adipocytes has been suggested as a promising strategy to combat obesity and its comorbidities [20]. Some browning agents like rosiglitazone [21] and isoproterenol [22] have potent browning activities, but associated with hepatotoxicity and cardiac toxicity in animal studies. Mirabegron, a β3 adrenergic receptor agonist, induces weight loss in rodents [23], but evidence is inconclusive regarding its effectiveness for increasing energy expenditure in clinical studies [24] and potential cardiovascular side effects [25] limit its application. Therefore, better approaches to combat obesity are greatly needed.

Trans-resveratrol (R), a browning compound, is a natural polyphenolic compound found in red grape skin, blueberries, raspberries, mulberries, and peanuts [26, 27]. Cell [28] and animal [29] studies suggest that R could induce beige adipocyte formation and its subsequent beneficial activities. The browning is achieved by enhancing mitochondria biogenesis and UCP-1 expression by activating AMP-activated protein kinase (AMPK), NAD-dependent deacetylase sirtuin 1 (SIRT1), peroxisome proliferator-activated receptor γ (PPARγ), and PPARγ coactivator α (PGC1-α) [30, 31]. SIRT1 deacetylates and further activates PPARγ, indirectly promoting browning of WAT. This modification also plays a key role in increasing PPARγ-binding activity and recruiting PRDM16 to PPARγ, which specifies brown adipogenic lineage transcriptional activity and initiates browning of WAT [32]. While limited human studies have suggested that R is beneficial to maintain metabolic health [33], the evidence regarding its browning effectiveness is inconclusive [34, 35], likely due to its low aqueous solubility (<0.1 mg/mL) [36], trivial bioavailability (peak plasma R concentration <10 μM after high-dose oral administration) [37], and no targeting specificity.

Author Manuscript Author Manuscript Author Manuscript Author Manuscript

Encapsulation of R in biocompatible nanoparticles comprised of soy phosphatidylcholine (PC), alpha-tocopherol acetate (αTA), and Kolliphor® HS15 can significantly enhance R's aqueous solubility, chemical stability, and dose-dependent expression of beige marker UCP-1 and CD137 in 3T3-L1 cells. N-(methylpolyoxyethylene oxycarbonyl)-1,2-distearoyl-sn-glycero-3-phosphoethanolamine (DSPE-PEG_{5000}) was further added to make R-encapsulated nanoparticles (Rnano) in this study. For targeted delivery, it was previously identified [38, 39] that a peptide CSWKYWFGEC from a library of cysteine-contained cyclic peptides can target ASCs via selectively binding to the glycanation site-deficient decorin (ΔDCN) receptor, a functional receptor expressed on the surface of WAT-resident ASCs in both rodents and humans [39]. Here, we designed a new linear ASC-targeting peptide (GSWKYWFGEGGC) that was crafted on the surface of Rnano, creating peptide ligand-coated Rnano (L-Rnano) (Fig. 1 A and B). The peptide was conjugated to the N-[(3-maleimide-1-oxopropyl) aminopropyl polyethyleneglycol-carbamyl] distearoylphosphatidyl-ethanolamine (DSPE-PEG_{5000}-maleimide) to form DSPE-PEG_{5000}-peptide, with maleimide on DSPE-PEG_{5000} reacted and coupled with the thiol group of cysteine (C) at the end of the peptide. DSPE and PC anchored onto the L-Rnano membrane by burying their two fatty acid tails inside the L-Rnano hydrophobic core of αTA and R, and the conjugated PEG_{5000}-peptide sections protruded outward to the aqueous environment, facilitating the selective binding to the ΔDCN receptor of ASCs. The PEG_{5000} can maintain L-Rnano's integrity and stability [40], and prolong their circulation by stabilizing them against opsonization and enzymatic degradation [41]. To the best of our knowledge, this is the first study to induce ASCs differentiating into beige adipocytes using the ASC-targeted L-Rnano.

Our experiments demonstrated that the ASC-targeted L-Rnano, compared to the non-targeted Rnano, had significantly higher binding affinity to and uptake by ΔDCN-transduced 3T3-L1 cells (ΔDCN cells), as well as higher ASC target specificity in obese C57BL/6J mice. We found that L-Rnano was 3.4-fold more efficient in targeting ASCs in mouse inguinal WAT (I-WAT) than Rnano. After biweekly intravenous administration of L-Rnano to high-fat diet (HFD)-induced obese C57BL/6J mice for five weeks, browning of I-WAT was induced, and obese mice lost 50% gonadal WAT (G-WAT) and 40% I-WAT, accompanied with improved glucose and cholesterol homeostasis, reduced inflammation, and no obvious toxicities. These results suggest that the ASC-targeted nanoparticle delivery of browning agents could be a transformative technology in combating obesity and its comorbidities.

2. Material and methods

2.1. Chemicals and reagents

R was purchased from Cayman Chemical Co., (Ann Arbor, MI, USA). αTA, cholesterol, bovine serum albumins (BSA), type 1 collagenase, β-glucuronidase from *Helix pomatia* (Type H-3), sulfatase from *Helix pomatia* (Type H-1), quercetin and anti-UCP-1 antibody were purchased from Sigma-Aldrich Chemical Co., (St. Louis, MO, USA). Soy PC and 1,2-dioleoyl-sn-glycero-3-phosphoethanolamine-N-(lissamine rhodamine B sulfonyl) (Rhoda) were purchased from Avanti Polar Lipids Inc. (Alabaster, AL, USA). Kolliphor® HS15 was offered as a gift from BASF Chemical Co. The ASC-targeting peptide

Author Manuscript Author Manuscript Author Manuscript Author Manuscript

(GSWKYWFGEGGC) was synthesized by GenScript USA Inc. (Piscataway, NJ, USA). DSPE-PEG_{5000}-maleimide and DSPE-PEG_{5000} (SUNBRIGHT®) were purchased from NOF Corporation (Tokyo, Japan). DiD was purchased from Thermo Fisher Scientific Co. (San Jose, CA, USA). Antibodies (PE anti-mouse CD34, Brilliant Violet 421™ anti-mouse CD31, Brilliant Violet 421™ anti-mouse CD45, Alexa Fluor® 594 anti-mouse CD29 and LEGENDplex™ mouse inflammation panel kit were purchased from Biolegend (San Diego, CA, USA). TRIzol® reagent. Maxima First Strand cDNA Synthesis Kit and PowerUp SYBR™ Green Master Mix were purchased from Thermo Scientific (Pittsburgh, PA, USA). Vectastain ABC kit was purchased from Vector Laboratories (Burlingame, CA, USA). ΔDCN-transduced 3T3-L1 cells (ΔDCN cells) were a gift from Dr. Mikhail G. Kolonin (The University of Texas Health Science Center at Houston, TX, USA).

2.2. Preparation and characteristics of nanoparticles

2.2.1. Preparation of DSPE-PEG_{5000}-peptide conjugate—

DSPE-PEG_{5000}-maleimide and the ASC targeting peptide were dissolved at an equal molar ratio in deionized water. The reaction mixture was gently stirred with a magnetic stirrer at room temperature for 24 hours. After the reaction, DSPE-PEG_{5000}-maleimide, the ASC targeting peptide and the DSPE-PEG_{5000}-peptide conjugate were characterized by matrix-assisted laser desorption ionization time of flight mass spectrometry (MALDI-TOF) (Applied Biosystems, Framingham, MA).

2.2.2. Preparation of nanoparticles—

A mixture composed of 4 mg R, 7 mg soy PC, 22 mg Kolliphor® HS15, 22 mg αTA, and DSPE-PEG_{5000} (replacing 5 mol% of PC) was dissolved in ethanol. After mixing, ethanol was removed using a nitrogen evaporator. The Rnano lipid mixture was then suspended in warm deionized water and homogenized and sonicated to get Rnano. L-Rnano was prepared by replacing DSPE-PEG_{5000} with equal molar mass of DSPE-PEG_{5000}-peptide. Vnano and L-Vnano were synthesized using the same materials and procedures but without R. For the *in vitro* binding experiment, fluorescence dye Rhoda (replacing 1 mol% of total PC) was added to make Rhoda-labeled nanoparticles. For the *in vivo* imaging and flow cytometer experiments, near-infrared fluorescent dye 1,1'-dioctadecyl-3, 3, 3', 3'-tetramethylindodicarbocyanine, 4-chlorobenzenesulfonate salt (DiD) (replacing 1 mol% of total PC) was added to make DiD-labeled nanoparticles. The prepared nanoparticles were passed through 100kDa Amicon Ultra centrifugal filter (Millipore, Billerico, MA) to eliminate free R, dye, peptide, or other compounds.

2.2.3. Characteristics of nanoparticles—

The particle size and polydispersity indexes (PI) were measured using a Brookhaven BI-MAS particle size analyzer, and the zeta potential was measured using a Zeta PALS analyzer (Brookhaven Corporation, NY). The morphology and size of nanoparticles were determined using a 200kV Hitachi H-8100 transmission electron microscopy (TEM) instrument (Tokyo, Japan). R concentrations, encapsulation efficiency and loading capacity were measured as follows: one volume of Rnano or L-Rnano was dissolved in 9 volumes of methanol, and the total R concentrations (Ctotal) in the Rnano or L-Rnano solution were measured using a Shimadzu high performance liquid chromatography (HPLC) system equipped with two LC-20AD solvent

Author Manuscript Author Manuscript Author Manuscript Author Manuscript

delivery units, a SIL-20AC HT autosampler, and a SPD-M20A photo diode array (PDA) detector (Shimadzu scientific instruments, Inc., Japan) with a C18 reverse-phase column (Symmetry® C18, 3.5 μm, 4.6×75 mm). The mobile phase was composed of methanol/water/acetic acid (50/50/0.5, v/v/v) with a flow rate of 1 mL/min. The detection wavelength was 310 nm. Free (non-encapsulated) R was separated from nanoencapsulated R using an ultrafiltration method (Millipore Amicon Ultra-15), and its concentrations were measured by the HPLC system (Cfree). To calculate the loading capacity, a certain volume of Rnano or L-Rnano (V) was dried using a vacuum freeze-drying system (Labconco, Kansas City, MO). The weight of dried Rnano or L-Rnano was expressed as WNANO. The encapsulation efficiency and loading capacity of R in the Rnano or L-Rnano were calculated according to the following equations, respectively:

$$\text{Encapsulation efficiency} = (\text{Ctotal} - \text{Cfree})/\text{Ctotal} \times 100\%$$
$$\text{Loading capacity} = (\text{CtotalV} - \text{CfreeV})/\text{WNANO} \times 100\%$$

2.2.4. Nanoparticle *in vitro* release study—The *in vitro* release behavior was measured in dissolution medium composed of 1×phosphate buffer saline (1×PBS, pH=7.4) and methanol (80:20, v:v) using a dialysis method. Free R, Rnano or L-Rnano containing 0.5 mg of R were dissolved and dispersed in 1 mL of dissolution medium and then placed in three different dialysis bags with MWCO 6,000–8,000. The entire dissolution medium was replaced with fresh pre-warmed medium every 2 hours. R concentrations in the dissolution media was measured using the HPLC system as described in the measurement of R encapsulation efficiency.

2.3. *In vitro* binding and uptake of nanoparticles

2.3.1. ΔDCN and 3T3-L1 cell culture—3T3-L1 cells (ATCC® CL-173™) were grown in cell culture media (Dulbecco's modified Eagle's medium containing 10% calf serum and 1x penicillin-streptomycin antibiotics) at 37°C, 95% humidity, and an atmosphere of 5% CO_2. cells were grown in the same conditions but with 5 μg/mL puromycin added in the media.

2.3.2. Mouse primary stromal vascular fraction isolation and culture—The WAT depots were weighed and rinsed in isolation buffer, and minced. The minced WAT was digested by Type 1 collagenase. Digested WAT was filtered through 100 μm nylon mesh (Spectrum, Rancho Dominquez, CA) to get a single cell suspension. After centrifugation at 800 × g for 10 minutes, floating mature adipocytes were removed and the pellets of the stromal vascular fraction (SVF) were collected and washed twice with the isolation buffer. After counting, SVF cells were plated into 6-well plates with DMEM growth media containing 10% fetal bovine serum (FBS, Atlas biological, CO). After 24 hours, unattached cells were removed by extensive washing with 1×PBS. The attached cells were cultured in the same medium and medium was changed every other day until cells reached 70–80% confluence.

2.3.3. Fluorescence microscopy of nanoparticle binding to cells—The fluorescence intensity of Rhoda-labeled Rnano and L-Rnano was equalized using a BioTek

Author Manuscript Author Manuscript Author Manuscript Author Manuscript

ELx800™ absorbance microplate reader (Winooski, VT) before treating cells to deliver an equivalent mass of nanoparticles. Primary murine SVF cells were cultured and grown to 80% confluency prior to treatment. ΔDCN cells or 3T3-L1 cells were cultured overnight prior to treatment. Cells were treated with Rhoda-labeled Rnano or L-Rnano at either 4°C or 37°C for 2 hours. Cells were then washed three times with ice-cold 1×PBS and fixed with 3.7% formaldehyde, followed by washing with ice-cold 1×PBS three times. After staining nuclei with 4′, 6-diamidine-2′-phenylindole dihydrochloride (DAPI), cells were mounted with Vectashield and visualized using an EVOS® auto fluorescence microscope (20× magnification) (AMG, Bothell, WA). Rhoda-labeled Rnano and L-Rnano were imaged in red (λ_{exc}: 560 nm, λ_{em}: 583 nm). Cell nuclei were stained by DAPI (λ_{exc}: 358 nm, λ_{em}: 461 nm) and shown in blue. For equal comparison of all images, the exposure times were identical for all measurements for each fluorophore.

2.3.4. Flow cytometry of nanoparticle binding to cells—Before treating cells, DiD amounts in DiD-labeled Rnano and L-Rnano was measured and diluted to ensure that both Rnano and L-Rnano contained equal DiD amounts. Adherent cells were trypsinized, resuspended at a density of 1×10^5 cells/mL and treated with DiD-labeled Rnano and L-Rnano for 2 hours at 200 rpm in a 37°C water bath. Cells were then centrifuged at 500 × g at 4°C for 5 minutes and the supernatant was removed. Cells were washed with 1×PBS followed by centrifugation at 500 × g at 4°C for 5 minutes. After removing the supernatant, cells were resuspended with a flow buffer (1×PBS containing 1% bovine serum albumin), and analyzed on a 4-laser Attune Nxt flow cytometer (ThermoFisher, USA).

2.3.5. Cellular R content—ΔDCN cells and primary mouse SVF cells were treated with free R, Rnano, or L-Rnano containing 0.1 and 1 mg/mL of R, respectively at 4°C or 37°C for 4 hours. Cells were then washed three times with ice-cold 1×PBS and collected in 0.6 M acetic acid in a glass tube. Ethyl acetate containing quercetin (internal standard) were added to the cell suspension and fully mixed, followed by sonication and centrifugation at 500 × g at 4°C for 5 minutes. The ethyl acetate fraction was collected and dried in a nitrogen evaporator. The residue was resuspended in methanol followed by injection and R detection using the HPLC system as described in the measurement of R encapsulation efficiency. The protein precipitates were dried using a nitrogen evaporator, and then digested using 0.5 N NaOH. After overnight incubation, cellular protein was quantified using a bicinchoninic acid (BCA) kit. Cellular R content was expressed as μg R/mg cellular protein.

2.4. Biodistribution and ASC targeting specificity of nanoparticles in mice

2.4.1. Biodistribution of nanoparticles in mice—Male 6-week old C57BL/6J mice purchased from the Jackson Laboratory were fed an HFD (45% energy from fat, D12451, Research Diets, Inc, New Brunswick, NJ) for 4 weeks. Randomized mice were matched by body weight (each pair of mice had similar body weight for receiving DiD-labeled Rnano and L-Rnano). The final injection volume was calculated based on body weight (injection volume was “5 μL/g body weight”). DiD-labeled Rnano or L-Rnano were injected into mice via tail veins. After 24 hours, mice were imaged using a IVIS® spectrum *in vivo* imaging system (IVIS). Mice were then sacrificed and perfused from the left ventricle with

Author Manuscript Author Manuscript Author Manuscript Author Manuscript

1×PBS. The liver, BAT, retroperitoneal WAT (RP-WAT), I-WAT and G-WAT were collected. Fluorescence images of the organs were observed using the IVIS system.

2.4.2. ASC targeting specificity of nanoparticles in mice—After IVIS imaging, RP-WAT, I-WAT and G-WAT were enzymatically digested and SVF was resuspended in the flow buffer as described above for flow cytometry. After centrifugation of digested tissues at 500 × g at 4°C for 5 minutes, floating mature adipocytes were collected, washed twice with the flow buffer and kept on ice. The SVF pellet was washed, and red blood cells (RBC) were lysed in 1×RBC lysis buffer (Biolegend, San Diego, CA). After washing and centrifugation at 500 × g at 4°C for 5 minutes, SVF cells were counted and resuspended in flow buffer at 1×10^7 cells/mL. SVF cells were stained on ice for 30 minutes with the following fluorophore-conjugated antibodies with optimal dilution: PE anti-mouse CD34, Brilliant Violet 421™ anti-mouse CD31, Brilliant Violet 421™ anti-mouse CD45 and Alexa Fluor® 594 anti-mouse CD29, protected from light. The cells were pelleted, washed twice with flow buffer, resuspended in flow buffer and analyzed using the Attune NxT flow cytometer. Gating strategies are shown as follow. First, the SVF population was identified by size using FSC and SSC. Second, the $CD45^-/CD31^-/CD34^+$ events were gated from the SVF population. Third, populations of ASC ($CD45^-/CD31^-/CD34^+/CD29^+$) were gated and the percentage of DiD^+ ASCs was determined from this population. Relative ASC target specificity of L-Rnano compared to Rnano.

2.5. Animal study

Sixty male, 6-week old C57BL/6J mice from Jackson's Laboratory (Bar Harbor, ME) were fed the HFD for 9 weeks. Mice were maintained at a standard condition, and had access to water and the HFD diet *ad libitum*. After 4 weeks, body weight and composition of mice were measured, and they were randomly assigned into one of the following six treatment groups: saline; void nanoparticles (Vnano); ligand-Vnano (L-Vnano); free R; Rnano; and L-Rnano. All treatments were dissolved into saline and administered to mice via tail vein injection twice a week for additional 5 weeks (from week 5 to 9). The R dose was 52.5 mg/kg body weight/injection (15 mg/kg body weight/day). Food intake and body weight were recorded weekly. During the last two weeks, glucose tolerance test (GTT) and insulin tolerance test (ITT) were conducted, and the cold tolerance test was performed at 4°C for 6 hours. Mice were then fasted overnight and humanely euthanized with CO_2 inhalation followed by cervical dislocation. Blood was collected from the abdominal vein, and serum and plasma were obtained by centrifugation. Brain, liver, lung, spleen, kidneys, skeletal muscle, BAT, RP-WAT, I-WAT and G-WAT of each mouse were collected, measured, weighed and described in detail. Each tissue was cut into 3 pieces to be immediately frozen in liquid nitrogen followed by storage at −80°C or fixed in 4% paraformaldehyde (for histology), or stored in RNAlater™ solution. The animal protocol was approved by the animal care and use committee of Texas Tech University, Lubbock, TX.

2.5.1. Body composition—Body composition of mice was measured at week 0, 2, 4 and 5 of injection treatments using an EchoMRI™ whole body composition Analyzer (EchoMRI LLC, Houston, TX).

Author Manuscript Author Manuscript Author Manuscript Author Manuscript

2.5.2. Cold tolerance test—Initial rectal temperature was measured before placing the mice into a cold room (4 ± 1°C). Rectal temperature was measured by inserting a thermometer 1 cm deep into the rectum. The rectal probe was wiped with alcohol swabs (70% isopropyl alcohol) and coated with glycerol between uses. Mice were housed individually in a cage without bedding in the cold room. Mice had free access to food and water. Mice were kept in the cold room for 6 hours and the rectal temperature was measured hourly.

2.5.3. Measurement of plasma lipid profile, insulin and glucose concentrations—Serum concentrations of total cholesterol and low-density lipoprotein cholesterol (LDL-C) were measured using an AU400 clinical chemistry analyzer with enzymatic reagents (Beckman Coulter, Inc.) at the Jean Mayer USDA Human Nutrition Research Center on Aging at Tufts University, Boston, MA. Fasting plasma glucose concentrations were measured by One Touch® glucometer. Fasting insulin concentrations were determined by ELISA using a commercial kit (Millipore, Billerica, MA). The insulin resistance was evaluated using homeostatic model assessment for insulin resistance (HOMA-IR) by the following formula:

$$\text{HOMA-IR} = [\text{Fasting plasma glucose (mg/dL)} \times \text{Fasting plasma insulin (mU/L)}] \times (405)^{-1}$$

2.5.4. Measurement of WAT R content—I-WAT and G-WAT (around 100 mg) were homogenized in 1 mL saline. Quercetin and 1 mL ethyl acetate were added into the homogenates followed by vortexing for 1 minute. After centrifugation at 1,500 × g for 10 min at 4°C, the upper phase was transferred into a new tube, and dried under nitrogen. The dried extract was reconstituted with methanol and subsequently measured by the HPLC system as described in the measurement of R encapsulation efficiency.

2.5.5. Measurement of liver R content—Liver (around 100 mg) was weighed and homogenized in 1 mL of saline. After adding β-glucuronidase and sulfatase from helix pomatia into the homogenized liver, the mixture was incubated at 37°C for 2 hours to convert R derivatives to free R. Quercetin and 1 mL of ethyl acetate were added, and the mixture was vortexed followed by centrifugation at 1,500 × g for 10 min at 4°C. R was extracted and measured as described above.

2.5.6. Real-time PCR—Total RNA was extracted from I-WAT using a TRIzol® reagent and cDNA was synthesized from quantified RNA using a Maxima First Strand cDNA Synthesis Kit according to the manufacturer's instructions. cDNA levels of target genes were measured using PowerUp SYBR™ green master mix on a real-time PCR system (Eppendorf Mastercycler® ep realplex instrument, NY). The mRNA-fold changes were calculated using the $2^{-\Delta\Delta Ct}$ method, which were normalized against the housekeeping gene 36B4. Primer sequences of target genes are listed in Table S3.

2.5.7. Immunohistochemistry staining—The formalin-fixed I-WAT was embedded in paraffin and cut into 5 μm sections by the Department of Pathology of Texas Tech University Health Sciences Center (TTUHSC). Deparaffinized and rehydrated sections were

Author Manuscript Author Manuscript Author Manuscript Author Manuscript

incubated with the anti-UCP-1 antibody overnight at 4°C. After washing, they were then incubated with biotinylated secondary antibody for 1 hour. The sections were developed utilizing avidin-conjugated horseradish peroxidase with diaminobenzidine as a substrate using a Vectastain ABC kit according to the manufacturer's instructions. Following the development, the slides were mounted under coverslips and images were taken using the EVOS® auto fluorescence microscope.

2.5.8. Hematoxylin and eosin (H&E) staining—H&E staining of I-WAT was conducted by the Department of Pathology of TTUHSC. Briefly, the paraffin-embedded I-WAT sections (5 μm) were deparaffinized and rehydrated with xylene and ethanol. Sections were cleaned with water to remove reagent residues, blotted to remove excess water, and then incubated with Hematoxylin for 4 minutes, washed several times using water. The sections were stained with Eosin and dehydrated. Finally, sections were cleaned and covered with a xylene-based mounting medium.

2.5.9. Histological evaluation and serum chemistry profile—Five mice from each group were randomly selected for safety evaluation. After terminal exsanguinations under isoflurane, the heart, liver, lungs, kidneys, skeletal muscle, brain, and spleen of each mouse were collected, fixed, embedded, sectioned, and stained for histological examination and evaluation. The serum chemistry profiles were measured. The assays were conducted by the pathologists who were not directly involved in the study at the Texas A&M Veterinary Medical Diagnostic Laboratory at College Station, Texas.

2.6. Statistical analysis

Data analysis was performed using statistical software "R". In order to compare multiple group means, one-way ANOVA followed by Tukey HSD Post Hoc test was conducted. To compare two group means, two-tailed Student's *t*-test was conducted. Data are expressed as mean ± standard error of the mean. Differences were considered statistically significant at $p < 0.05$.

3. Results and discussion

3.1. Development and characterization of nanoparticles

In the present study, we developed ASC-targeted nanoparticles by incorporating the ASC-targeting peptide on their surface (Fig. 1B). While a cyclic version of this peptide (CSWKYWFGEC) has been identified [42], we reasoned that the steric effects of a cyclic form [43] might interfere with nanoparticle incorporation. Therefore, we modified and redesigned a linear ASC-targeting peptide (GSWKYWFGEGGC) and validated the peptide conjugation by MALDI-TOF. The spectrum of DSPE-PEG_{5000}-peptide exhibited an average mass at m/z 6963, while the peptide alone showed a single and sharp peak at m/z 1376 (Fig. 1B). The mass difference between DSPE-PEG_{5000}-peptide and peptide was matched the mass of DSPE-PEG_{5000}-maleimide (Fig. 1B). This confirms that the peptide was successfully conjugated to form DSPE-PEG_{5000}-peptide, which can be incorporated to L-Rnano with the ASC-targeting peptide protruding outward.

Author Manuscript Author Manuscript Author Manuscript Author Manuscript

The nanoparticle composition was optimized for particle size, stability, encapsulation efficiency, binding to ΔDCN cells, and WAT targeting in mice (Table S1, Fig. S1A). From these data, a weight ratio of PC: αTA: Kolliphor® HS15: R = 7:22:22:4 was selected for further use. Kolliphor® HS15 has been selected as a surfactant, which is required in nanoparticle preparation, to form the stable nanostructure by decreasing the surface tension of the nanoparticle [44]. Additionally, Kolliphor® HS15 [45] and PEG_{5000} helped maintain the integrity and colloidal stability of Rnano and L-Rnano [46]by protecting them from enzyme-induced degradation and nonspecific adsorption of blood proteins [47]. R's aqueous solubility was greatly increased by loading into nanoparticles (Fig. 1C). While 1 mg of free R did not dissolve in 1 mL of 1×PBS at room temperature, Rnano and L-Rnano containing the same amount of R had a translucent state with visible opalescence (Fig. 1C). The TEM images of Rnano and L-Rnano indicated that they were spherical shape nanoparticles with a size of 90–110 nm (Fig. 1C). L-Rnano was slightly larger than Rnano due to the presence of the conjugated ASC-targeting peptide on their surface (Fig. 1D). The PI of freshly made Rnano and L-Rnano were measured to be 0.315 ± 0.020 and 0.341 ± 0.020, respectively (Fig. 1D). Both Rnano and L-Rnano had negative surface charges and their zeta potentials were −19.88 ± 2.30 and −10.37 ± 1.90, respectively (Fig. 1D). Importantly, Rnano and L-Rnano had a high R encapsulation efficiency of 95.8 ± 0.2% and 96.2 ± 0.4%, respectively. Nevertheless, the loading capacity of L-Rnano (22.3 ± 0.6%) was lower than that of Rnano (29.2 ± 0.8%) due to the extra mass of the targeting peptide. The physical stability of Rnano and L-Rnano at different temperatures was assessed, as presented in Fig. S2.

The *in vitro* R release pattern from Rnano and L-Rnano compared to free R was measured using a dialysis method. Free R exhibited a burst release pattern with 35% of free R released within the first 2 hours (Fig. 1E). Rnano and L-Rnano released only 10% of R within the first 2 hours. The free R was continuously released in the following 6 hours, and then became undetectable. In contrast, both Rnano and L-Rnano exhibited a similar sustained release pattern at a release rate about 5% per hour, a much improved release manner over free R.

3.2. L-Rnano target ΔDCN-expressing cells in vitro

The target efficacy of L-Rnano was next assessed using ΔDCN cells and primary mouse SVF cells. L-Rnano were designed to bind to and then internalized by ΔDCN cells, while they have no target efficacy at 3T3-L1 cells that do not express the ΔDCN receptor (Fig. 2A). Compared to Rnano, higher binding and uptake of fluorescent dye (Rhoda)-labeled L-Rnano in ΔDCN cells at both 37 and 4°C and no differences in 3T3L1 cells were clearly observed by a fluorescence microscope. Fig. 2B showed representative images from each treatment, temperature and cell line. These data indicated that the binding and uptake of L-Rnano is mediated by homing to the ΔDCN receptor. L-Rnano's target effect was confirmed by flow cytometry as well. After treating ΔDCN cells with DiD-labeled Rnano or L-Rnano, 20% and 95% of ΔDCN cells became DiD positive (DiD+, blue color), respectively (Fig. 2C). To further investigate that nanoparticles bind and uptake by ΔDCN cells is an active, temperature-dependent process, the cellular R content of cells treated with free R, Rnano and L-Rnano at both 37 and 4°C were measured. Cellular R content in ΔDCN

Author Manuscript Author Manuscript Author Manuscript Author Manuscript

cells treated with L-Rnano compared to free R or Rnano was 2.3- and 1.6-fold higher at 37°C, and 2.3- and 2.0-fold higher at 4°C, respectively (Fig. 2D). This result was consistent with fluorescent data, in which the binding and uptake effect of Rhoda-labeled L-Rnano was higher than Rnano at both 37 and 4°C resulting in an enhanced fluorescent intensity (Fig. 2B). Additionally, compared to 37°C, cellular R content among all treatments were lower at 4°C, indicating that free R and nanoparticles were taken up by ΔDCN cells via a temperature-dependent transport mechanism.

Binding and uptake of L-Rnano by primary mouse SVF cells isolated from I-WAT of C57BL/6J mice were also determined using the above methods. Mouse SVF cells bound more L-Rnano than Rnano at both 37°C and 4°C (Fig. 2E). However, SVF cells bound less L-Rnano than ΔDCN cells (Fig. 2B and E). Loss of surface ΔDCN receptor expression on ASCs after overnight culture of SVF cells and presence of endothelial cells and other heterogeneous population in the SVF could partially contribute to the low binding affinity [48]. Consistent with the cellular R content in ΔDCN cells, L-Rnano-treated compared to free R and Rnano-treated SVF cells had 2.5- and 1.5-fold higher cellular R content at 37°C, respectively, and 2.8- and 2.1-fold higher cellular R content at 4°C, respectively (Fig. 2F). In summary, above data indicate that ASC-targeted L-Rnano had a higher binding affinity to ΔDCN-expressing cells and delivered more R into these cells than non-targeted Rnano.

3.3. L-Rnano target ASCs in mice

The ASC target specificity of L-Rnano was determined using flow cytometry in C57BL/6J mice. After intravenous injection of DiD-labeled Rnano or L-Rnano into the mice, the biodistribution and intensity of Rnano and L-Rnano in mice and WAT depots were visualized using the IVIS system. The higher DiD intensity indicates a higher target level of the nanoparticles. After sacrificing mice, WAT depots were collected and digested. SVF cells were isolated by fractionation, and labeled with antibodies. ASCs were identified as CD45−CD31−/CD34+CD29+ [49], and DiD fluorescence signals in ASCs reflect binding and uptake of Rnano or L-Rnano by these cells (Fig. 3A).

L-Rnano had greater accumulation in I-WAT, G-WAT and RP-WAT than Rnano in mice *in situ* (Fig. 3B). Among these WAT depots, I-WAT had the highest L-Rnano fluorescence signals (Fig. 3B). DiD signal intensity in I-WAT isolated from L-Rnano-treated mice was 1.8-fold higher ($p<0.05$) than that of Rnano-treated mice. Meanwhile, liver DiD signal intensity was 1.2-fold lower in L-Rnano-treated mice compared to Rnano-treated mice (Fig. 3B, Fig. S3). These data indicate that L-Rnano targeted WAT, especially I-WAT in mice. The ASC target specificity of L-Rnano in I-WAT and G-WAT was then measured. L-Rnano targeted ASCs, because the percentage of DiD+ ASCs was 3.4-fold (from I-WAT, $p<0.05$), and 2.3-fold (from G-WAT) higher in L-Rnano-treated than Rnano-treated mice (Fig. 3C, Fig. S4). Moreover, mature adipocytes were collected from I-WAT and G-WAT of these mice, and nanoparticle uptake data indicated that the percentage of DiD+ adipocytes in both I-WAT and G-WAT isolated from L-Rnano-treated mice was lower than that of Rnano-treated mice (Fig. 3D). In addition, the percentage of DiD+ endothelial (CD31+), and hematopoietic (CD45+) was similar in Rnano-treated and L-Rnano-treated mice. These results demonstrate that L-Rnano targeted ASCs, especially I-WAT-derived ASCs.

Author Manuscript Author Manuscript Author Manuscript Author Manuscript

3.4. L-Rnano reduce obesity in HFD-induced obese C57BL/6J mice

Based on the bioavailability of R [50, 51], we selected 15 mg/kg body weight/day of R dose to investigate the anti-obesity efficacy of L-Rnano. To avoid targeting peptide digestion in the gastrointestinal tract, obese C57BL/6J mice maintained on the HFD were given intravenous injection of free R, Rnano, L-Rnano, or their respective controls: saline, Vnano) or L-Vnano twice per week for five weeks. Food intake was similar among six groups (Fig. 4A). During the 5-week treatment period, mice treated with saline, Vnano, L-Vnano or free R gained body weight and had increased percentage of body fat (% body fat) (Fig. 4A). Compared to free R-treated mice, Rnano-treated and L-Rnano-treated mice had 6% and 13% lower body weight, and 1.5- and 2-fold lower % body fat, respectively (Fig. 4A), indicating the high anti-obesity efficacy of L-Rnano. Lean mass was similar among six groups. L-Rnano-treated mice had the highest % body lean because they had the lowest body weight (Fig. 4A). These changes in % body fat were associated with significantly lower masses of G-WAT (1.9-fold, $p<0.05$), I-WAT (1.6-fold, $p<0.05$) (Fig. 4B), and RP-WAT (2.2-fold, $p<0.001$) (Fig. S5) in L-Rnano-treated versus free R-treated mice. The representative images of G-WAT and I-WAT were shown in Fig. S6. After H&E staining of I-WAT sections, the average adipocyte size in I-WAT from Rnano- or L-Rnano-treated mice was significantly 1.6- and 3.3-fold smaller than that of free R-treated mice (Fig. 4C). Importantly, I-WAT from L-Rnano-treated mice showed multilocular lipid droplet morphology (arrows in Fig. 4C), a general characteristic of brown and beige adipocytes. These data suggest that L-Rnano induced beige adipocyte formation in I-WAT in obese C57BL/6J mice.

To validate browning effects of L-Rnano, a cold tolerance test was conducted. Compared with the other groups of mice, L-Rnano-treated mice maintained their body temperature more efficiently during an acute cold challenge ($p=0.07$, area under the curve (AUC)) (Fig. 4D). Especially at the end of the test (hour 6), L-Rnano-treated mice still maintained their core temperature at 37.6°C, whereas the body temperature of mice in the other groups dropped to ~36.8°C. The enhanced thermogenesis during cold exposure correlated with increased UCP-1 mRNA and protein levels in I-WAT of L-Rnano-treated mice (Fig. 4E). L-Rnano-treated mice had 23.8-, 14.8-, and 6.0-fold higher I-WAT UCP-1 mRNA levels ($p<0.05$) than mice treated with saline, free R and Rnano, respectively (Fig. 4E). L-Rnano also promoted the mRNA expression of beige adipocyte marker CD137 in I-WAT (Fig. S7A). Previous studies have suggested that different WAT depots may have different browning potentials. The lack of difference in UCP-1 mRNA expression in G-WAT across our six treatment groups (Fig. S7B) confirmed that I-WAT was more responsive to browning agents than G-WAT [52]. Increased UCP-1 expression and browning of I-WAT likely account for the improved thermogenesis during cold exposure in mice. Our data strongly suggest that L-Rnano enhanced the formation of beige adipocytes in mouse I-WAT, which correlated with reduced body weight and fat mass, and increased thermogenesis.
To determine R delivery efficacy to I-WAT, we next measured R content in I-WAT, G-WAT and the liver. I-WAT R content was 4.2- ($p<0.05$) and 3.1-fold ($p<0.05$) higher in L-Rnano-treated compared to free R- and Rnano-treated mice, respectively (Fig. 4F). There were no significant differences in G-WAT R content among free R, Rnano and L-Rnano groups (Fig. 4F). L-Rnano delivered 2.8-fold more R to I-WAT than G-WAT (Fig. 4F). Meanwhile, L-Rnano delivered less R to the liver than both free R and Rnano (Fig. 4F).

Author Manuscript Author Manuscript Author Manuscript Author Manuscript

L-Rnano-treated mice had 37.0- ($p<0.001$) and 7.8-fold ($p<0.001$) lower liver R content than free R-treated and Rnano-treated mice, respectively (Fig. 4F). These data indicate that as L-Rnano delivered more R to I-WAT, less R was accumulated in the liver.

The liver is a major organ that accumulates and metabolizes circulating free R [53]. Even through free R-treated mice had the highest liver R content, most of R might be metabolized via methylation, glucuronidation, sulfation and oxidative degradation in the liver [54]. Nanoencapsulation reduces liver accumulation of R [55, 56]. In this study, hydrophilic PEG on the surface of both Rnano and L-Rnano maintained their integrity and stability by protecting them from enzymatic degradation [57]. PEG might also prolong their circulation time by stabilizing them against opsonization through decreasing interactions with hepatocytes and mononuclear phagocyte system cells. All these contributed to reduction of R accumulation in the liver and elimination from the circulation, which further promote the target delivery of R to ASCs in I-WAT. When less nanoparticles are taken up by the liver, the circulation time of the nanoparticles is prolonged. The prolonged circulation time will also promote the target delivery of nanoparticles to desired tissues or cells. In this study, liver fluorescence signal intensity was lower in L-Rnano-treated mice compared to Rnano-treated mice (Fig. 3B). Consistent with the image data, L-Rnano-treated mice had 37.0- ($p<0.001$) and 7.8-fold ($p<0.001$) lower liver R content than free R-treated and Rnano-treated mice, respectively (Fig. 4F). The data indicated that both PEGlated Rnano and L-Rnano had longer circulation time and less uptake by the liver. Additionally, I-WAT R content was 4.2- ($p<0.05$) and 3.1-fold ($p<0.05$) higher in L-Rnano-treated compared to free R-treated and Rnano-treated mice, respectively (Fig. 4F). Since L-Rnano-treated mice compared to other groups of mice had significantly lower liver R content and higher I-WAT R content, it demonstrated that PEGlation worked well in prolonging L-Rnano circulation, and peptide ligands on the L-Rnano also enhanced ASC targeted delivery. These data indicated that the potential influence of the protein corona profile of Rnano and L-Rnano in plasma may have few impacts on the prolonged circulation efficacy of PEG_{5000}. More experiments are guaranteed in this research area in the future. In addition, obese mice have enhanced permeability and retention in WAT [58], which likely further increased retention of Rnano and L-Rnano. With their ASC-targeting capability, L-Rnano delivered more R to G-WAT and I-WAT than Rnano. Hence, L-Rnano-treated mice had lowest liver R content, which is consistent with our *in vivo* target specificity data using DiD-labeled Rnano and L-Rnano. We conducted major organ necropsies and histological analysis, and measured the mice plasma levels of aspartate aminotransferase, alanine aminotransferase and total bilirubin, which are standard biomarkers used to assess liver damage (Table S2). Although no significant differences were observed among all treatments, reduced L-Rnano accumulation in the liver predicts that it has low hepatic toxicity.

3.5. L-Rnano improve metabolic health

With reduced fat mass by L-Rnano-induced browning of I-WAT, obesity-related insulin resistance, inflammation and hypercholesterolemia could also be improved. In this study, L-Rnano-treated compared to saline-treated mice had significantly lower fasting plasma insulin and glucose concentrations (Fig. 5A). Furthermore, both Rnano and L-Rnano groups had significantly 1.3- and 1.8-fold lower HOMA-IR as compared to the saline group (Fig.

Author Manuscript Author Manuscript Author Manuscript Author Manuscript

5A). However, no significant differences were found in GTT and ITT assays among 6 treatment groups. The HFD in this study might result in abundant fat and fatty acids in the body, which act as the main substrates (rather than glucose) utilized by beige adipocytes in I-WAT. For better understanding, hyperinsulinemic euglycemic glucose clamps [59] could be used in future studies.

Rnano-treated and L-Rnano-treated mice also had 1.5- and 2.7-fold lower plasma leptin concentrations when compared to free R-treated mice, respectively, and similar changes in I-WAT leptin mRNA levels among six groups (Fig. 5B). Recent studies demonstrated that activating I-BAT improved cholesterol metabolism by accelerating hepatic clearance of cholesterol-rich remnant lipoproteins [60] and promoting high-density lipoprotein (HDL) reverse cholesterol transport [61]. In this study, L-Rnano-treated mice had the lowest serum concentrations of total cholesterol and LDL-C among six groups of mice (Fig. 5C), suggesting that browning I-WAT may enhance cholesterol clearance.

Furthermore, L-Rnano reduced inflammation. The excessive expansion of WAT in obesity leads to macrophage infiltration, and macrophages count can increase from 5% to 60% of total WAT cells [62]. TNF-α, IL-6, MCP-1 and other inflammatory cytokines and chemokines are secreted by macrophages, adipocytes, and other types of cells in WAT. Increased inflammatory response is known to be associated with insulin resistance and cardiovascular disease [63, 64]. It has been reported that R decreases inflammatory cytokine production from adipocytes and macrophages [30]. Consistently, we found that, in parallel to the lowest WAT weight and smallest adipocytes size, L-Rnano-treated mice had a 2-fold reduction in plasma concentrations of TNF-α, IL-6, interferon gamma (IFN-γ), and MCP-1, as compared to other groups of mice (Fig. S8A). Macrophage infiltration into I-WAT was assessed by F4/80 mRNA expression, which was decreased by L-Rnano (Fig. S8B). Overall, browning of I-WAT not only decreased body weight and fat mass, but also improved glucose and cholesterol homeostasis, and reduced inflammation, which may have beneficial effects on type 2 diabetes, cardiovascular disease, and other obesity-related diseases and disorders.

3.6. Safety evaluation

To evaluate the safety of Rnano and L-Rnano, serum chemistry and histological examinations of studied mice were conducted. No significant differences were found in the serum chemistry, including renal function, electrolytes, liver function and other basic metabolic panels among six groups (Table S2). In heart and aorta samples, adipose tissue adjacent to the aorta showed moderate lymphocyte infiltration in saline-treated mice. A small number of foam cells were found in alveolar spaces of lungs, and in the liver, and a small number of hepatocytes had expanded cytoplasm in a few mice among the six treatment groups. These histopathologic manifestations are commonly observed in healthy mice and not consider to be related to treatments. There were no representative differences between saline and the other treatments (Fig. S9).

4. Conclusion

The *de novo* differentiation of ASCs into beige adipocytes has been considered as a very intriguing strategy in combating obesity, but its practical application has been retarded due

Author Manuscript Author Manuscript Author Manuscript Author Manuscript

to the low delivery efficiency of browning agents to ASCs, and high toxicity of browning agents. Targeted delivery could be the solution to deliver enough browning agents to ASCs while avoiding their side effects and toxicity. To this end, we developed an ASC-targeted nanoparticle structure by crafting a peptide on the nanoparticle, which can selectively bind to the ΔDCN receptor on the surface of WAT-resident ASCs. To test the targeted delivery capability and verify the possibility of browning, R as the active load was encapsulated in the nanoparticle in this study. Indeed, nanoencapsulation and targeting delivery significantly enhanced R's solubility, release profile, circulation time, and particularly ASC targeting efficiency and uptake. Our data showed that the ASC-targeted L-Rnano, compared to the non-targeted Rnano, had significantly higher binding affinity to and uptake by ΔDCN cells, as well as higher ASC target specificity in HFD-induced obese C57BL/6J mice, L-Rnano was more than 3-fold more efficient in targeting ASCs in mouse I-WAT than Rnano, while keeping a minimum liver accumulation with low hepatic toxicity. After biweekly intravenous administration of L-Rnano to the mice for only five weeks, targeted R delivery had already significantly induced ASCs differentiation into beige adipocytes, evidenced by significantly increased UCP-1 expression in I-WAT. Strikingly, this browning of I-WAT resulted in obese mice losing 50% G-WAT and 40% I-WAT, accompanied with improved glucose and cholesterol homeostasis, reduced inflammation, and no obvious toxicities. These data unambiguously demonstrate that browning of subcutaneous WAT is feasible, and this browning approach will not only enhance thermogenesis to significantly reduced body weight and fat mass, but also improve metabolic health.

In this study, a representative browning agent R was encapsulated in our ASC-targeted nanoparticles. Since a broad range of browning agents could also be encapsulated in this ASC-targeted nanoparticle structure that may have synergistic effects on treating obesity with high efficacy and low toxicity, this ASC-targeted nanoparticle delivery system could be a transformative technology in combating obesity and its comorbidities. It is also envisioned that this ASC-targeted nanoparticle delivery system, when encapsulating other agents, may induce ASCs differentiation into other types of cells, and find applications in tissue repair, regenerative medicine and therapy of other diseases.

Supplementary Material

Refer to Web version on PubMed Central for supplementary material.

Acknowledgements

We thank Mary Catherine Hastert for taking transmission electron microscopy images of nanoparticles, Dr. Jie Liu and Shahjalal Md Khan for assisting the animal study, and the College of Arts & Sciences Microscopy (TTU, Lubbock, TX) for use of their facilities. The project described was supported by Grant Number 1R15AT008733 and 1R15AT010395 from the National Center for Complementary and Integrative Health, and Grant Number 19AIREA34480011 and 16SDG30200001 from American Heart Association. The content is solely the responsibility of the authors and does not necessarily represent the official views of the National Institutes of Health and American Heart Association. Additional financial support was provided by and the Harry E. Bovay, Jr. Foundation, TTU Obesity Research Cluster, and the U.S. Department of Agriculture, Agriculture Research Service under Specific Cooperative Agreement #58-1950-4-003.

Author Manuscript Author Manuscript Author Manuscript Author Manuscript

References

[1]. Hales CM, Carroll MD, Fryar CD, Ogden CL, Prevalence of obesity among adults and youth: United States, 2015–2016, 2017.

[2]. Goktas Z, Owens S, Boylan M, Syn D, Shen C-L, Reed DB, San Francisco S, Wang S, Associations between tissue visfatin/nicotinamide, phosphoribosyltransferase (Nampt), retinol binding protein-4, and vaspin concentrations and insulin resistance in morbidly obese subjects, Mediators Inflamm., 2013 (2013).

[3]. Betz MJ, Enerbäck S, Targeting thermogenesis in brown fat and muscle to treat obesity and metabolic disease, Nature Reviews Endocrinology, 14 (2018) 77.

[4]. Villarroya F, Cereijo R, Villarroya J, Giralt M, Brown adipose tissue as a secretory organ, Nature Reviews Endocrinology, 13 (2017) 26.

[5]. Goktas Z, Moustaid-Moussa N, Shen C-L, Boylan M, Mo H, Wang S, Effects of bariatric surgery on adipokine-induced inflammation and insulin resistance, Front. Endocrinol. (Lausanne), 4 (2013) 69. [PubMed: 23772224]

[6]. Yoneshiro T, Aita S, Matsushita M, Kayahara T, Kameya T, Kawai Y, Iwanaga T, Saito M, Recruited brown adipose tissue as an antiobesity agent in humans, The Journal of clinical investigation, 123 (2013) 3404–3408. [PubMed: 23867622]

[7]. Blondin DP, Tingelstad HC, Noll C, Frisch F, Phoenix S, Guérin B, Turcotte ÉE, Richard D, Haman F, Carpentier AC, Dietary fatty acid metabolism of brown adipose tissue in cold-acclimated men, Nature communications, 8 (2017) 14146.

[8]. Kajimura S, Spiegelman BM, Seale P, Brown and beige fat: physiological roles beyond heat generation, Cell Metab, 22 (2015) 546–559. [PubMed: 26445512]

[9]. Villarroya F, Cereijo R, Gavaldà-Navarro A, Villarroya J, Giralt M, Inflammation of brown/beige adipose tissues in obesity and metabolic disease, Journal of internal medicine, 284 (2018) 492–504. [PubMed: 29923291]

[10]. Porter C, Herndon DN, Chondronikola M, Chao T, Annamalai P, Bhattarai N, Saraf MK, Capek KD, Reidy PT, Daquinag AC, Human and mouse brown adipose tissue mitochondria have comparable UCP1 function, Cell metabolism, 24 (2016) 246–255. [PubMed: 27508873]

[11]. Virtanen KA, Lidell ME, Orava J, Heglind M, Westergren R, Niemi T, Taittonen M, Laine J, Savisto N-J, Enerbäck S, Functional brown adipose tissue in healthy adults, New England Journal of Medicine, 360 (2009) 1518–1525.

[12]. Leitner BP, Huang S, Brychta RJ, Duckworth CJ, Baskin AS, McGehee S, Tal I, Dieckmann W, Gupta G, Kolodny GM, Mapping of human brown adipose tissue in lean and obese young men, Proceedings of the National Academy of Sciences, 114 (2017) 8649–8654.

[13]. Rogers NH, Brown adipose tissue during puberty and with aging, Annals of medicine, 47 (2015) 142–149. [PubMed: 24888388]

[14]. Min SY, Kady J, Nam M, Rojas-Rodriguez R, Berkenwald A, Kim JH, Noh H-L, Kim JK, Cooper MP, Fitzgibbons T, Human'brite/beige'adipocytes develop from capillary networks, and their implantation improves metabolic homeostasis in mice, Nature medicine, 22 (2016) 312.

[15]. Harms M, Seale P, Brown and beige fat: development, function and therapeutic potential, Nature medicine, 19 (2013) 1252.

[16]. Wang QA, Tao C, Gupta RK, Scherer PE, Tracking adipogenesis during white adipose tissue development, expansion and regeneration, Nature medicine, 19 (2013) 1338.

[17]. Tang W, Zeve D, Suh JM, Bosnakovski D, Kyba M, Hammer RE, Tallquist MD, Graff JM, White fat progenitor cells reside in the adipose vasculature, Science, 322 (2008) 583–586. [PubMed: 18801968]

[18]. Wu J, Boström P, Sparks LM, Ye L, Choi JH, Giang A-H, Khandekar M, Virtanen KA, Nuutila P, Schaart G, Beige adipocytes are a distinct type of thermogenic fat cell in mouse and human, Cell, 150 (2012) 366–376. [PubMed: 22796012]

[19]. Sacks H, Symonds ME, Anatomical locations of human brown adipose tissue: functional relevance and implications in obesity and type 2 diabetes, Diabetes, 62 (2013) 1783–1790. [PubMed: 23704519]

Author Manuscript Author Manuscript Author Manuscript Author Manuscript

[20]. Tseng Y-H, Cypess AM, Kahn CR, Cellular bioenergetics as a target for obesity therapy, Nature reviews Drug discovery, 9 (2010) 465–482. [PubMed: 20514071]

[21]. Forman LM, Simmons DA, Diamond RH, Hepatic failure in a patient taking rosiglitazone, Annals of internal medicine, 132 (2000) 118–121. [PubMed: 10644272]

[22]. CHANDER HASS YADAV M, KHANAM R, Isoproterenol toxicity induced ECG alterations in wistar rats: role of histamine H3 receptor agonist imetit, IJPPS, 6 (2014) 23–33.

[23]. Hao L, Scott S, Abbasi M, Zu Y, Khan MSH, Yang Y, Wu D, Zhao L, Wang S, Beneficial metabolic effects of mirabegron in vitro and in high-fat diet-induced obese mice, Journal of Pharmacology and Experimental Therapeutics, 369 (2019) 419–427.

[24]. Chondronikola M, The role of brown adipose tissue and the thermogenic adipocytes in glucose metabolism: recent advances and open questions, Current Opinion in Clinical Nutrition & Metabolic Care, 23 (2020) 282–287. [PubMed: 32412979]

[25]. Cypess AM, Weiner LS, Roberts-Toler C, Elía EF, Kessler SH, Kahn PA, English J, Chatman K, Trauger SA, Doria A, Activation of human brown adipose tissue by a β3-adrenergic receptor agonist, Cell metabolism, 21 (2015) 33–38. [PubMed: 25565203]

[26]. Burns J, Yokota T, Ashihara H, Lean ME, Crozier A, Plant foods and herbal sources of resveratrol, J. Agric. Food. Chem, 50 (2002) 3337–3340. [PubMed: 12010007]

[27]. Hurst WJ, Glinski JA, Miller KB, Apgar J, Davey MH, Stuart DA, Survey of the trans-resveratrol and trans-piceid content of cocoa-containing and chocolate products, J. Agric. Food. Chem, 56 (2008) 8374–8378. [PubMed: 18759443]

[28]. Zu Y, Overby H, Ren G, Fan Z, Zhao L, Wang S, Resveratrol liposomes and lipid nanocarriers: Comparison of characteristics and inducing browning of white adipocytes, Colloids and Surfaces B: Biointerfaces, 164 (2018) 414–423. [PubMed: 29433059]

[29]. Wang S, Liang X, Yang Q, Fu X, Rogers CJ, Zhu M, Rodgers B, Jiang Q, Dodson MV, Du M, Resveratrol induces brown-like adipocyte formation in white fat through activation of AMP-activated protein kinase (AMPK) α1, International Journal of Obesity, 39 (2015) 967. [PubMed: 25761413]

[30]. Wang S, Moustaid-Moussa N, Chen L, Mo H, Shastri A, Su R, Bapat P, Kwun I, Shen C-L, Novel insights of dietary polyphenols and obesity, J. Nutr. Biochem, 25 (2014) 1–18. [PubMed: 24314860]

[31]. Tennen RI, Michishita-Kioi E, Chua KF, Finding a target for resveratrol, Cell, 148 (2012) 387–389. [PubMed: 22304906]

[32]. Qiang L, Wang L, Kon N, Zhao W, Lee S, Zhang Y, Rosenbaum M, Zhao Y, Gu W, Farmer SR, Brown remodeling of white adipose tissue by SirT1-dependent deacetylation of Pparγ, Cell, 150 (2012) 620–632. [PubMed: 22863012]

[33]. Berman AY, Motechin RA, Wiesenfeld MY, Holz MK, The therapeutic potential of resveratrol: a review of clinical trials, NPJ precision oncology, 1 (2017) 35. [PubMed: 28989978]

[34]. Barger JL, An adipocentric perspective of resveratrol as a calorie restriction mimetic, Annals of the New York Academy of Sciences, 1290 (2013) 122–129. [PubMed: 23855474]

[35]. Poulsen MM, Jorgensen J, Jessen N, Richelsen B, Pedersen SB, Resveratrol in metabolic health: an overview of the current evidence and perspectives, Ann. N.Y. Acad. Sci, 1290 (2013) 74–82. [PubMed: 23855468]

[36]. Bonechi C, Martini S, Ciani L, Lamponi S, Rebmann H, Rossi C, Ristori S, Using liposomes as carriers for polyphenolic compounds: the case of trans-resveratrol, PLoS One, 7 (2012) e41438. [PubMed: 22936976]

[37]. Wenzel E, Somoza V, Metabolism and bioavailability of trans-resveratrol, Molecular nutrition & food research, 49 (2005) 472–481. [PubMed: 15779070]

[38]. Daquinag AC, Zhang Y, Amaya-Manzanares F, Simmons PJ, Kolonin MG, An isoform of decorin is a resistin receptor on the surface of adipose progenitor cells, Cell stem cell, 9 (2011) 74–86. [PubMed: 21683670]

[39]. Daquinag AC, Dadbin A, Snyder B, Wang X, Sahin AA, Ueno NT, Kolonin MG, Non-glycanated Decorin is a drug target on human adipose stromal cells, Molecular Therapy-Oncolytics, 6 (2017) 1–9. [PubMed: 28607949]

Author Manuscript Author Manuscript Author Manuscript Author Manuscript

[40]. Heurtault B, Saulnier P, Pech B, Proust JE, Benoit JP, A novel phase inversion-based process for the preparation of lipid nanocarriers, Pharm Res, 19 (2002) 875–880. [PubMed: 12134960]

[41]. Owens DE III, Peppas NA, Opsonization, biodistribution, and pharmacokinetics of polymeric nanoparticles, International journal of pharmaceutics, 307 (2006) 93–102. [PubMed: 16303268]

[42]. Daquinag A, Tseng C, Salameh A, Zhang Y, Amaya-Manzanares F, Dadbin A, Florez F, Xu Y, Tong Q, Kolonin M, Depletion of white adipocyte progenitors induces beige adipocyte differentiation and suppresses obesity development, Cell death and differentiation, 22 (2015) 351. [PubMed: 25342467]

[43]. Kelly KA, Nahrendorf M, Amy MY, Reynolds F, Weissleder R, In vivo phage display selection yields atherosclerotic plaque targeted peptides for imaging, Molecular imaging and biology, 8 (2006) 201. [PubMed: 16791746]

[44]. Leonardi A, Bucolo C, Romano GL, Platania CBM, Drago F, Puglisi G, Pignatello R, Influence of different surfactants on the technological properties and in vivo ocular tolerability of lipid nanoparticles, International journal of pharmaceutics, 470 (2014) 133–140. [PubMed: 24792979]

[45]. Jokerst JV, Lobovkina T, Zare RN, Gambhir SS, Nanoparticle PEGylation for imaging and therapy, Nanomedicine, 6 (2011) 715–728. [PubMed: 21718180]

[46]. van Vlerken LE, Vyas TK, Amiji MM, Poly (ethylene glycol)-modified nanocarriers for tumor-targeted and intracellular delivery, Pharmaceutical research, 24 (2007) 1405–1414. [PubMed: 17393074]

[47]. Schlenoff JB, Zwitteration: coating surfaces with zwitterionic functionality to reduce nonspecific adsorption, Langmuir, 30 (2014) 9625–9636. [PubMed: 24754399]

[48]. Gimble JM, Bunnell BA, Chiu ES, Guilak F, Concise review: Adipose-derived stromal vascular fraction cells and stem cells: Let's not get lost in translation, Stem cells, 29 (2011) 749–754. [PubMed: 21433220]

[49]. Taha MF, Hedayati V, Isolation, identification and multipotential differentiation of mouse adipose tissue-derived stem cells, Tissue and Cell, 42 (2010) 211–216. [PubMed: 20483444]

[50]. Andlauer W, Kolb J, Siebert K, Fürst P, Assessment of resveratrol bioavailability in the perfused small intestine of the rat, Drugs under experimental and clinical research, 26 (2000) 47–55. [PubMed: 10894555]

[51]. Cottart CH, Nivet-Antoine V, Laguillier-Morizot C, Beaudeux JL, Resveratrol bioavailability and toxicity in humans, Molecular nutrition & food research, 54 (2010) 7–16. [PubMed: 20013887]

[52]. Wang W, Seale P, Control of brown and beige fat development, Nature reviews: Molecular cell biology, 17 (2016) 691. [PubMed: 27552974]

[53]. Alexis F, Pridgen E, Molnar LK, Farokhzad OC, Factors affecting the clearance and biodistribution of polymeric nanoparticles, Molecular pharmaceutics, 5 (2008) 505–515. [PubMed: 18672949]

[54]. Andres-Lacueva C, Macarulla MT, Rotches-Ribalta M, Boto-Ord ez M, Urpi-Sarda M, Rodríguez VM, Portillo MP, Distribution of resveratrol metabolites in liver, adipose tissue, and skeletal muscle in rats fed different doses of this polyphenol, Journal of agricultural and food chemistry, 60 (2012) 4833–4840. [PubMed: 22533982]

[55]. Kwon J-T, Hwang S-K, Jin H, Kim D-S, Minai-Tehrani A, Yoon H-J, Choi M, Yoon T-J, Han D-Y, Kang Y-W, Body distribution of inhaled fluorescent magnetic nanoparticles in the mice, Journal of occupational health, 50 (2008) 1–6.

[56]. Cho W-S, Cho M, Jeong J, Choi M, Han BS, Shin H-S, Hong J, Chung BH, Jeong J, Cho M-H, Size-dependent tissue kinetics of PEG-coated gold nanoparticles, Toxicology and applied pharmacology, 245 (2010) 116–123. [PubMed: 20193702]

[57]. Olbrich C, Müller R, Enzymatic degradation of SLN—effect of surfactant and surfactant mixtures, Int. J. Pharm, 180 (1999) 31–39. [PubMed: 10089289]

[58]. Hossen MN, Kajimoto K, Akita H, Hyodo M, Harashima H, Vascular-targeted nanotherapy for obesity: unexpected passive targeting mechanism to obese fat for the enhancement of active drug delivery, Journal of controlled release, 163 (2012) 101–110. [PubMed: 22982237]

[59]. DeFronzo RA, Tobin JD, Andres R, Glucose clamp technique: a method for quantifying insulin secretion and resistance, American Journal of Physiology: Endocrinology and Metabolism, 237 (1979) E214.

Author Manuscript Author Manuscript Author Manuscript Author Manuscript

[60]. Berbée JF, Boon MR, Khedoe PPS, Bartelt A, Schlein C, Worthmann A, Kooijman S, Hoeke G, Mol IM, John C, Brown fat activation reduces hypercholesterolaemia and protects from atherosclerosis development, Nature communications, 6 (2015) 6356.

[61]. Bartelt A, John C, Schaltenberg N, Berbée JF, Worthmann A, Cherradi ML, Schlein C, Piepenburg J, Boon MR, Rinninger F, Thermogenic adipocytes promote HDL turnover and reverse cholesterol transport, Nature communications, 8 (2017) 15010.

[62]. Weisberg SP, McCann D, Desai M, Rosenbaum M, Leibel RL, Ferrante AW, Obesity is associated with macrophage accumulation in adipose tissue, The Journal of clinical investigation, 112 (2003) 1796–1808. [PubMed: 14679176]

[63]. Gómez-Zorita S, Fernández-Quintela A, Lasa A, Hijona E, Bujanda L, Portillo MP, Effects of resveratrol on obesity-related inflammation markers in adipose tissue of genetically obese rats, Nutrition, 29 (2013) 1374–1380. [PubMed: 24012391]

[64]. Asghar A, Sheikh N, Role of immune cells in obesity induced low grade inflammation and insulin resistance, Cellular immunology, 315 (2017) 18–26. [PubMed: 28285710]

Author Manuscript Author Manuscript Author Manuscript Author Manuscript

Highlights

- Resveratrol-loaded targeted nanoparticles promote fat and weight loss.
- Resveratrol-loaded targeted nanoparticles improve metabolic health.
- Targeted delivery of resveratrol to adipose stromal cells induces beige adipocyte formation.
- Targeted nanoparticles bind to the delta decorin receptor on adipose stromal cells.
- Adipose stromal cells-targeted nanoparticles combat obesity and its comorbidities.

Author Manuscript Author Manuscript Author Manuscript Author Manuscript

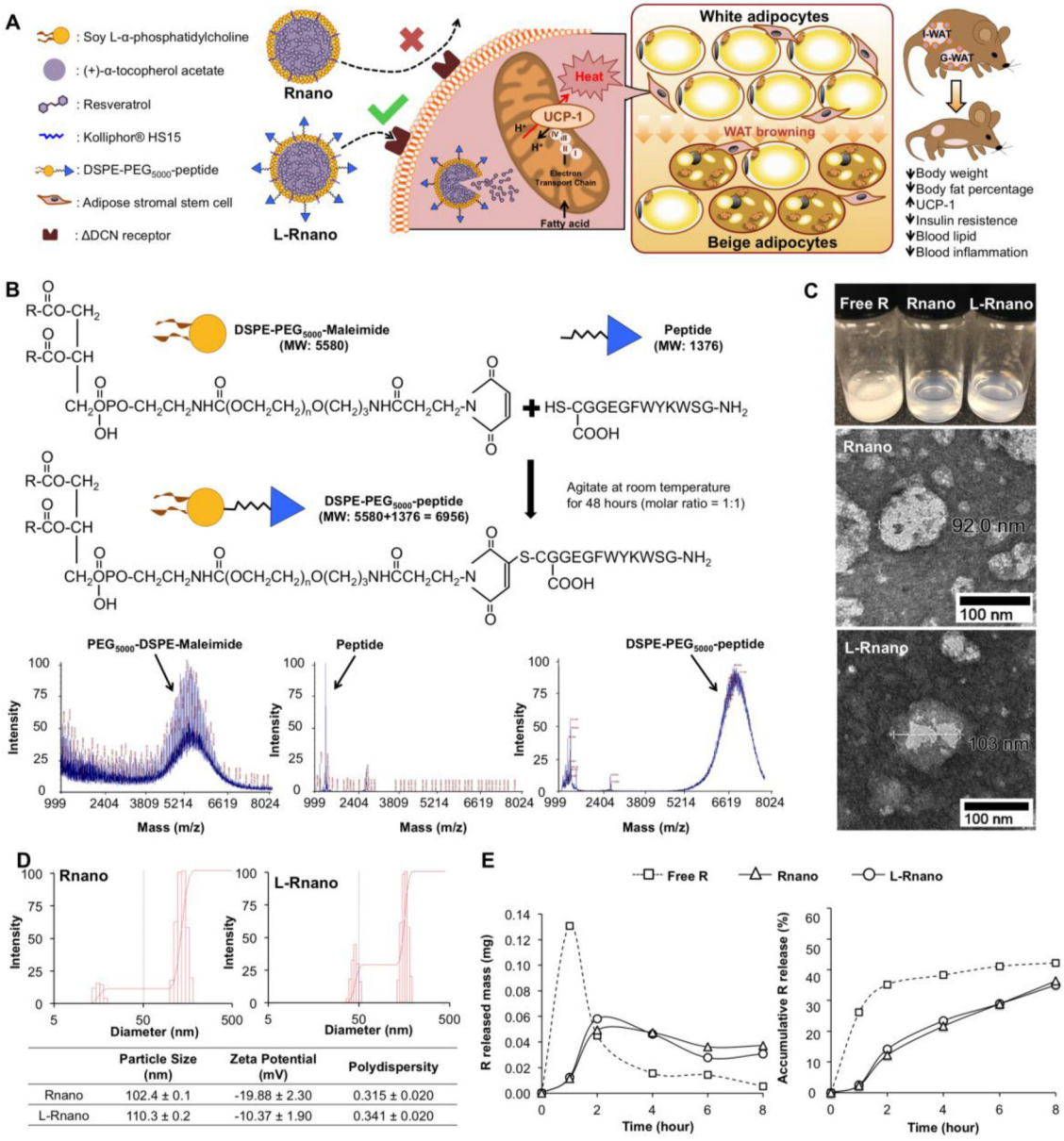

Fig. 1.

L-Rnano are designed to deliver R to ASCs. **(A)** Illustration of L-Rnano's targeting and working mechanisms. L-Rnano and Rnano are nanoparticles loaded with R. In contrast to Rnano, L-Rnano carry the ASC-targeting peptide ligand that has a high binding affinity to the ΔDCN receptor on the surface of ASCs. After internalization by the ASCs in subcutaneous WAT (I-WAT in mice), L-Rnano deliver R into the ASCs and induce their differentiation into beige adipocytes, subsequently resulting in browning of I-WAT, body fat loss, and improved metabolic health. **(B)** Conjugation reaction and MALDI-TOF chromatography of DSPE-PEG_{5000}-maleimide, ASC-targeting peptide and DSPE-PEG_{5000}-peptide. **(C)** Free R, Rnano and L-Rnano suspended in 1×PBS. TEM images of Rnano and L-Rnano. **(D)** Physical characteristics of Rnano and L-Rnano. **(E)** *In vitro* R release profiles

of free R, or Rnano, or L-Rnano. Data are calculated from three independent experiments and expressed as mean ± SEM.

Author Manuscript Author Manuscript Author Manuscript Author Manuscript

Author Manuscript Author Manuscript Author Manuscript Author Manuscript

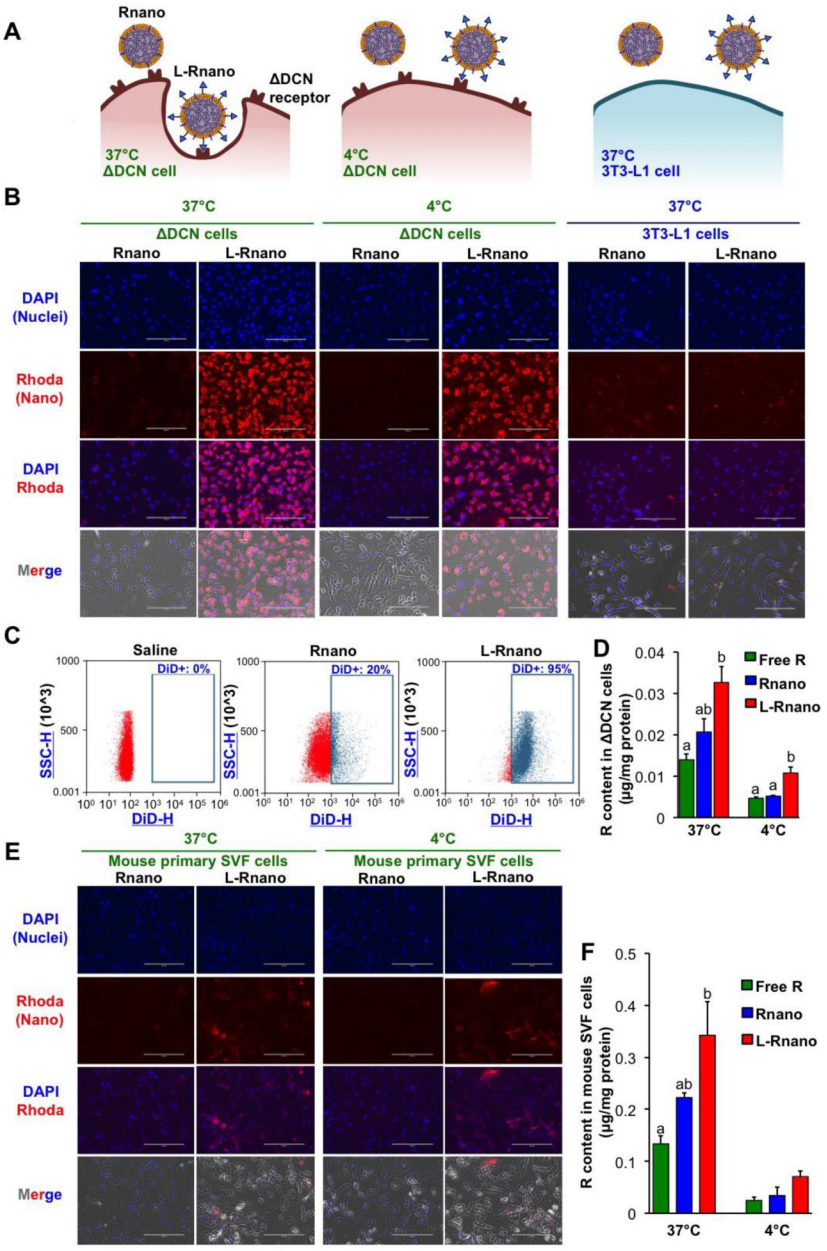

Fig. 2.

L-Rnano bind and deliver R to cells expressing the ΔDCN receptor *in vitro*. **(A)** Overview of the predicted binding and internalization of L-Rnano and Rnano at 4°C and 37°C in ΔDCN cells or 3T3-L1 cells. **(B)** The binding and uptake of Rhoda-labeled Rnano or L-Rnano (red) by ΔDCN or 3T3-L1 cells. **(C)** Flow cytometry analysis of binding and uptake of DiD-labeled Rnano or L-Rnano by ΔDCN cells. **(D)** Cellular R content in ΔDCN cells. **(E)** The binding and uptake of Rhoda-labeled Rnano or L-Rnano (red) by primary mouse SVF cells. **(F)** Cellular R content in primary mouse SVF cells. Scale bar = 200 μm. Data are calculated from three independent experiments and expressed as mean ± SEM. Bars without

a common superscript differ, $p<0.05$ by one-way ANOVA followed by Tukey HSD Post Hoc test.

Author Manuscript Author Manuscript Author Manuscript Author Manuscript

Author Manuscript Author Manuscript Author Manuscript Author Manuscript

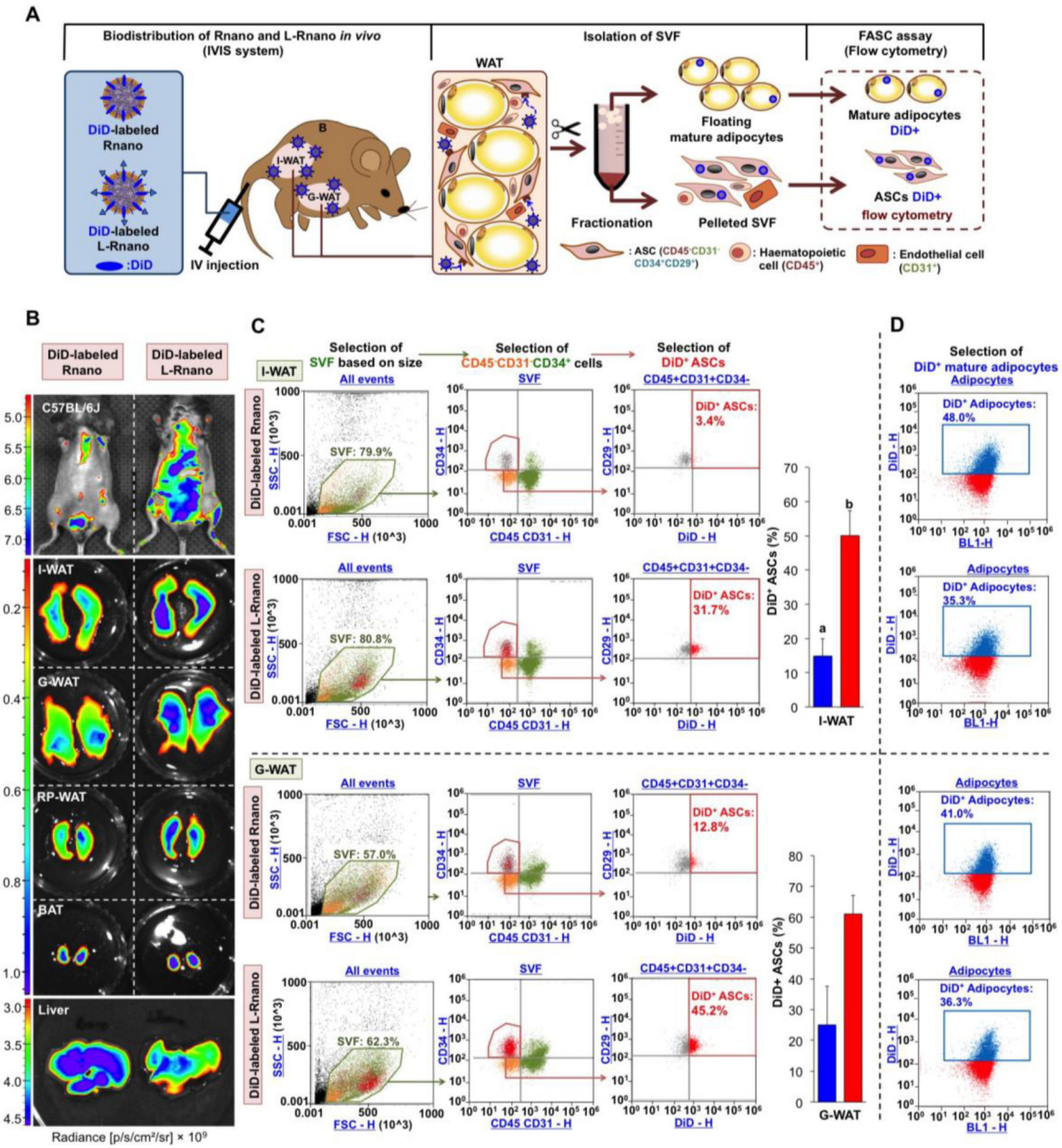

Fig. 3.

L-Rnano target WAT-derived ASCs in C57BL/6J mice. **(A)** Schematic of intravenous administration of Rnano and L-Rnano, SVF isolation, ASC identification, and quantification of DiD$^+$ ASCs and mature adipocytes. **(B)** IVIS images of mice, WAT depots, BAT and the liver after 24-hour post intravenous administration of DiD-labeled Rnano or L-Rnano. Radiance (p/s/cm^2/sr) is shown. Images are representatives of three independent experiments. **(C)** Binding and uptake of DiD-labeled Rnano or L-Rnano by ASCs in I-WAT or G-WAT was measured by flow cytometry. **(D)** Binding and uptake of DiD-labeled Rnano or L-Rnano by mature white adipocytes isolated from the I-WAT or G-WAT. Bars without a common superscript differ, $p<0.05$ by a two-tailed Student's *t*-test.

Author Manuscript Author Manuscript Author Manuscript Author Manuscript

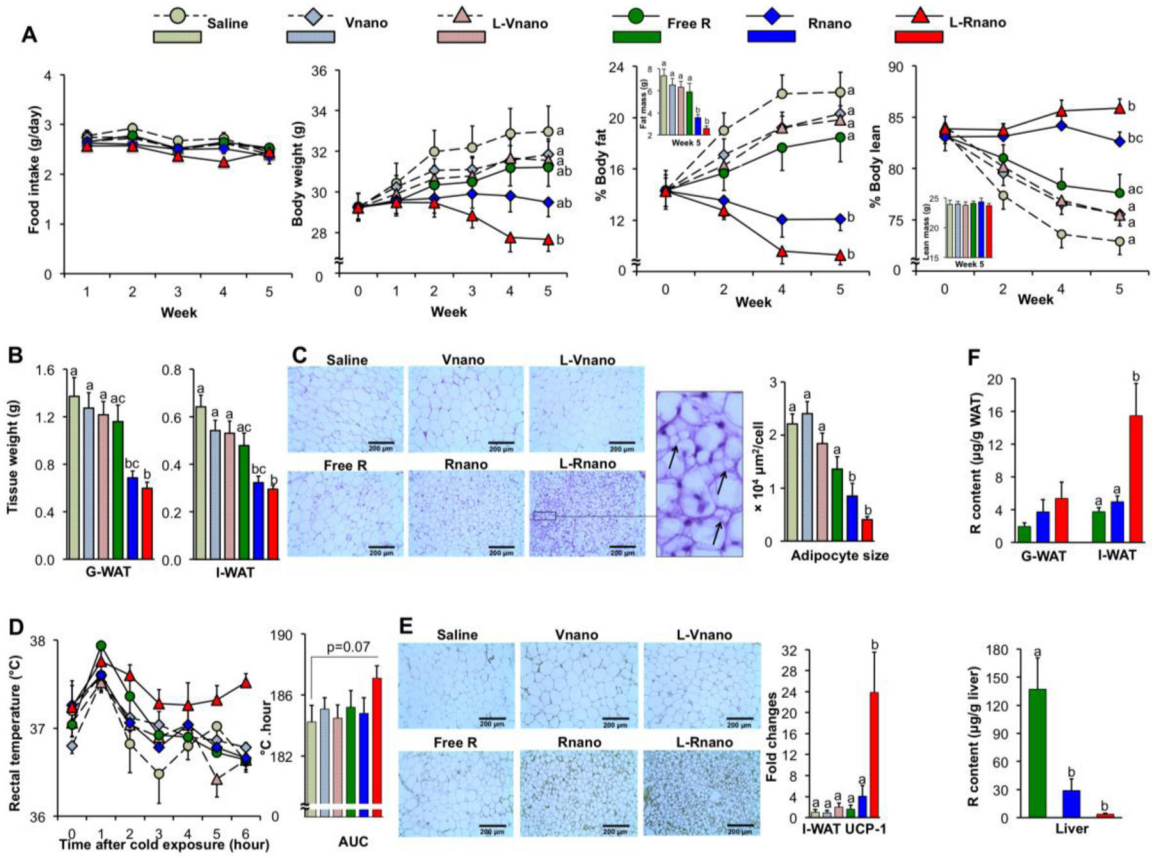

Fig. 4.

L-Rnano treat obesity via browning I-WAT in C57BL/6J mice. **(A)** Food intake, body weight, % body fat and % body lean of mice (n=10). **(B)** Weights of G-WAT and I-WAT. **(C)** Representative H&E histological images of I-WAT, and adipocyte sizes were quantified microscopically (n=5). Arrows show multilocular lipid droplet morphology in the I-WAT section of L-Rnano-treated mice. **(D)** Core body temperature changes over 6 hours of cold exposure (n=5). The temperature changes are displayed as the AUC. **(E)** Representative UCP-1 immunostaining images of I-WAT sections (n=5), UCP-1 mRNA expression levels in I-WAT (n=7). **(F)** R content in G-WAT, I-WAT and the liver (n=10). Scale bar = 200 μm. Data are expressed as mean ± SEM. Bars or lines without a common superscript differ, $p<0.05$ by one-way ANOVA followed by Tukey HSD Post Hoc test.

Author Manuscript Author Manuscript Author Manuscript Author Manuscript

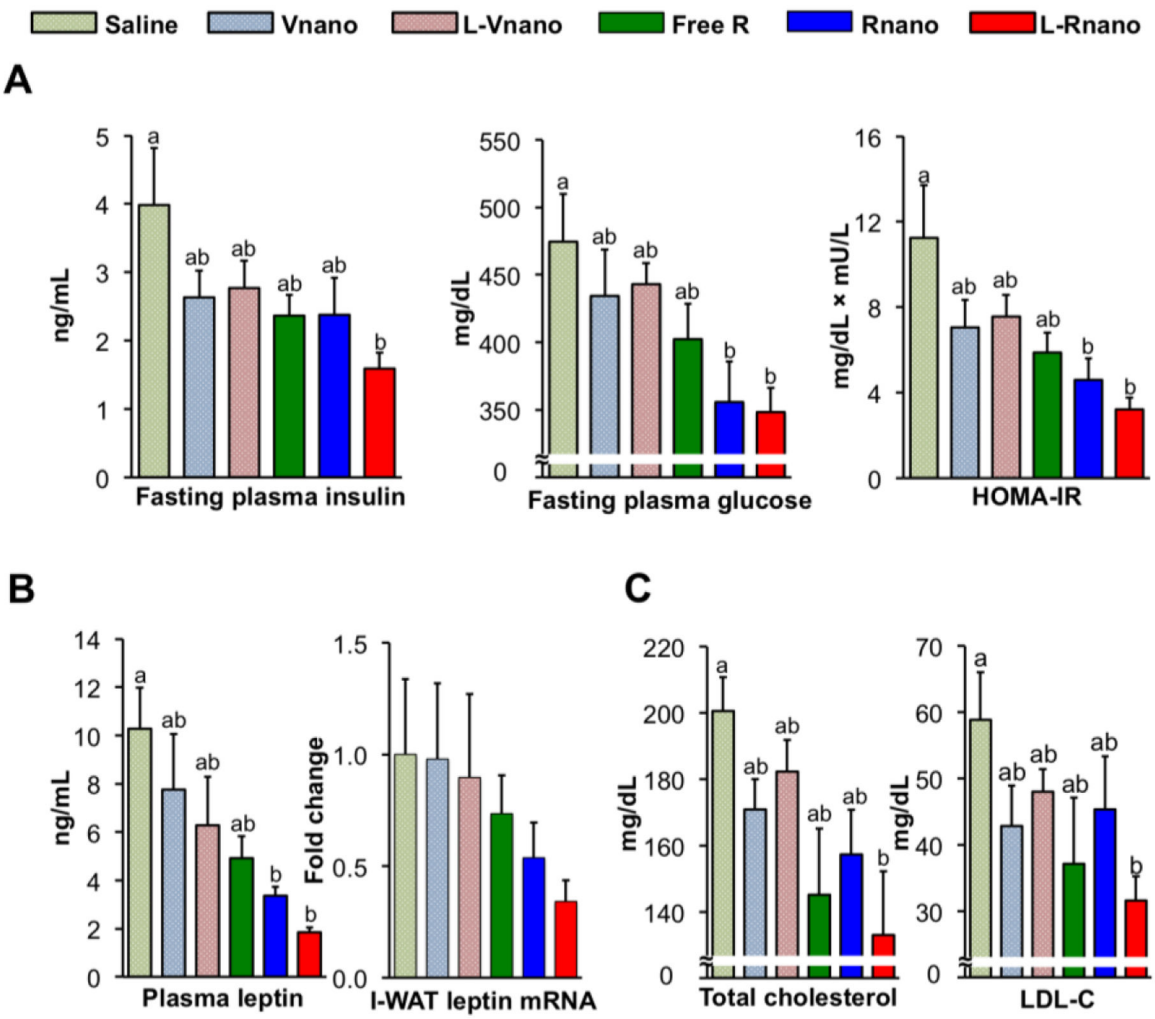

Fig. 5.

L-Rnano improve glucose and cholesterol homeostasis and decrease circulating leptin levels in C57BL/6J mice. **(A)** Fasting plasma insulin and glucose concentrations, and HOMA-IR (n=10). **(B)** Plasma leptin concentrations and leptin mRNA levels in I-WAT (n=10). **(C)** Blood total cholesterol and LDL-C concentrations (n=6). Data are expressed as mean ± SEM. Bars without a common superscript differ, $p<0.05$ by one-way ANOVA followed by Tukey HSD Post Hoc test.